



FULL-LENGTH PAPER

Crystal structure of SARS-CoV-2 nsp10–nsp16 in complex with small molecule inhibitors, SS148 and WZ16

Martin Klima¹ | Aliakbar Khalili Yazdi² | Fengling Li² | Irene Chau² | Taraneh Hajian² | Albina Bolotokova² | H. Ümit Kaniskan³ | Yulin Han³ | Ke Wang^{4,5} | Deyao Li^{4,5} | Minkui Luo^{4,5} | Jian Jin³ | Evzen Boura¹  | Masoud Vedadi^{2,6} 

¹Institute of Organic Chemistry and Biochemistry, Czech Academy of Sciences, Prague 6, Czech Republic

²Structural Genomics Consortium, University of Toronto, Toronto, Ontario, Canada

³Departments of Pharmacological Sciences and Oncological Sciences, Mount Sinai Center for Therapeutics Discovery, Tisch Cancer Institute, Icahn School of Medicine at Mount Sinai, New York, New York, USA

⁴Chemical Biology Program, Memorial Sloan Kettering Cancer Center, New York, New York, USA

⁶Program of Pharmacology, Weill Cornell Medical College of Cornell University, New York, New York, USA

⁵Department of Pharmacology and Toxicology, University of Toronto, Toronto, Ontario, Canada

Correspondence

Evzen Boura, Institute of Organic Chemistry and Biochemistry, Czech Academy of Sciences, v.v.i., 166 10 Prague 6, Czech Republic.
Email: evzen.boura@uochb.cas.cz

Masoud Vedadi, Department of Pharmacology and Toxicology, University of Toronto, Toronto, ON M5G 1L7, Canada.
Email: m.vedadi@utoronto.ca

Funding information

Czech Academy of Sciences, Grant/Award Number: RVO: 61388963; Chemical biology for drugging undruggable targets (ChemBioDrug), Grant/Award Number: CZ.02.1.01/0.0/0.0/16 019/0000729; European Regional Development Fund; University of Toronto COVID-19 Action Initiative-2020, and COVID-19 Mitacs Accelerate

Review Editor: John Kuriyan

Abstract

SARS-CoV-2 nsp10–nsp16 complex is a 2'-O-methyltransferase (MTase) involved in viral RNA capping, enabling the virus to evade the immune system in humans. It has been considered a valuable target in the discovery of antiviral therapeutics, as the RNA cap formation is crucial for viral propagation. Through cross-screening of the inhibitors that we previously reported for SARS-CoV-2 nsp14 MTase activity against nsp10–nsp16 complex, we identified two compounds (SS148 and WZ16) that also inhibited nsp16 MTase activity. To further enable the chemical optimization of these two compounds towards more potent and selective dual nsp14/nsp16 MTase inhibitors, we determined the crystal structure of nsp10–nsp16 in complex with each of SS148 and WZ16. As expected, the structures revealed the binding of both compounds to S-adenosyl-L-methionine (SAM) binding pocket of nsp16. However, our structural data along with the biochemical mechanism of action determination revealed an RNA-dependent SAM-competitive pattern of inhibition for WZ16, clearly suggesting that binding of the RNA first may help the binding of some SAM competitive inhibitors. Both compounds also showed some degree of selectivity against human protein MTases, an indication of great potential for chemical optimization towards more potent and selective inhibitors of coronavirus MTases.

KEYWORDS

COVID-19, nsp10, nsp16, SARS-CoV-2, SS148, WZ16

Martin Klima, Aliakbar Khalili Yazdi, and Fengling Li contributed equally to this study.

1 | INTRODUCTION

COVID-19 pandemic has been a grim reminder that viruses with pandemic potential can devastate human lives at any moment, and for a long time. As the development of vaccines takes a significant amount of time for each virus, prevention of future pandemics relies more on the discovery of antiviral therapeutics including pan inhibitors of enzymes crucial for viral replication. Two RNA methyltransferases (MTases), nsp14 and nsp16, are essential for coronaviral RNA cap formation that takes place in cytoplasm¹ to evade the human immune system.² Nsp14 is a bifunctional protein with a C-terminal MTase domain catalyzing N7-guanosine methylation and an N-terminal exoribonuclease domain.^{3–4} Nsp16 is a 2'-O-MTase, but it is only active when in complex with nsp10.^{5–6} These two MTases catalyze the transfer of methyl group from S-adenosyl-L-methionine (SAM) to the methyl acceptor substrates (RNA). We recently reported the full kinetic characterization of nsp14,⁷ and nsp16^{8,9} MTase activities, and inhibitors of nsp14 MTase activity.^{7,10} These included seven inhibitors that were identified through screening the severe acute respiratory syndrome coronavirus 2 (SARS-CoV-2) nsp14 *in vitro* against a collection of in-house synthesized 161 potential SAM competitive inhibitors.⁷

Nsp16 uses a cap-0 (N7-meGpppN RNA) as substrate and catalyzes the methylation of the ribose of the first nucleotide of mRNA at 2'-O position.^{11,12} This methylation requires a conserved K-D-K-E “catalytic tetrad” in substrate binding pocket.^{13,14} In fact, site-directed mutagenesis of these catalytic tetrad residues almost entirely blocked the MTase activity of the severe acute respiratory syndrome coronavirus (SARS-CoV) nsp16.^{15,16} RNA molecules with a non-methylated cap structure (Gppp-RNA) does not serve as a suitable substrate for nsp10–nsp16.¹⁷ Furthermore, it was shown that longer SARS-CoV RNAs, as well as synthetic N⁷-methylated small RNA substrates (5 nucleotides) could serve as effective substrates for this viral MTase complex.^{15,18}

Biochemical and structural studies have shown that nsp16 is active only in the presence of nsp10.^{15,17,19–22} It has been confirmed that nsp16 associates with nsp10 with a 1:1 M ratio and together they form a heterodimer, and this association is required for the binding of RNA substrate molecules with a cap-0 structure to nsp16.¹⁷ Further studies also postulated that the binding of nsp10 supports the SAM-binding of nsp16 subunit and would also extend the RNA binding pocket of nsp10–nsp16 complex.¹⁷ Nsp10 is a highly conserved zinc binding protein with around 99% identity in SARS-CoV and SARS-CoV-2.^{20–22} The interface between nsp16 and nsp10 subunits from SARS-CoV has been mapped using

mutagenesis, and the critical interactions for nsp16 MTase activity have been identified.^{16,23} Other mutational studies have also shown that targeting the interaction surface of nsp10–nsp16 complex completely abrogates the MTase activity of nsp16.¹⁷

Crystal structures of nsp10–nsp16 from SARS-CoV, the middle east respiratory syndrome coronavirus, and OC43-CoV, alone and in complex with substrates or ligands have provided critical information regarding the active site of this viral MTase complex.^{2,15–17,24} It has been shown that nsp16 forms a canonical SAM-dependent MTase fold.¹⁶ It adopts the seven-stranded β -sheet MTase fold, which forms two binding domains for SAM and methyl acceptor RNA substrate binding.¹⁶

Since the start of the COVID-19 pandemic, several crystal structures of nsp10–nsp16 from SARS-CoV-2 as apo, or in complex with RNA, SAM, or SAM analogs have been reported,^{25–27} which revealed a very high degree of structural conservation of nsp10–nsp16 complex among various coronavirus species. Combined with the importance of nsp10–nsp16 complex in coronavirus survival, this is a promising factor in design and development of pan-coronavirus antiviral small molecules.

Here, we report the cross-screening of nsp14 inhibitors against nsp10–nsp16 complex and the discovery of two dual nsp14/nsp16 inhibitors, SS148 and WZ16. Through structural and biochemical studies, we revealed an RNA-dependent SAM-competitive pattern of inhibition of nsp16 MTase activity. Potent dual inhibitors of nsp14/nsp16 could enable more efficient prevention of RNA cap formation in coronaviruses.

2 | RESULTS AND DISCUSSION

2.1 | Cross screening nsp14 MTase inhibitors against nsp10–nsp16 complex

Recently, we reported on the inhibition of SARS-CoV-2 nsp14 MTase activity by seven compounds we identified through screening of an in-house collection of 161 synthesized SAM competitive protein MTase inhibitors and SAM analogs.⁷ We hypothesized that possibly some of these compounds may also inhibit nsp10–nsp16 complex MTase activity, providing an opportunity to optimize them towards the development of more potent and selective nsp14–nsp16 dual inhibitors. We tested the seven compounds along with -S-adenosylhomocysteine (SAH) as a control using the previously reported optimized nsp10–nsp16 radiometric assay⁹ with compound concentrations ranging from 0.098 to 100 μ M. Interestingly, out of seven compounds, only SS148 and WZ16 showed significant nsp10–nsp16 inhibition with IC₅₀ values of 1.2

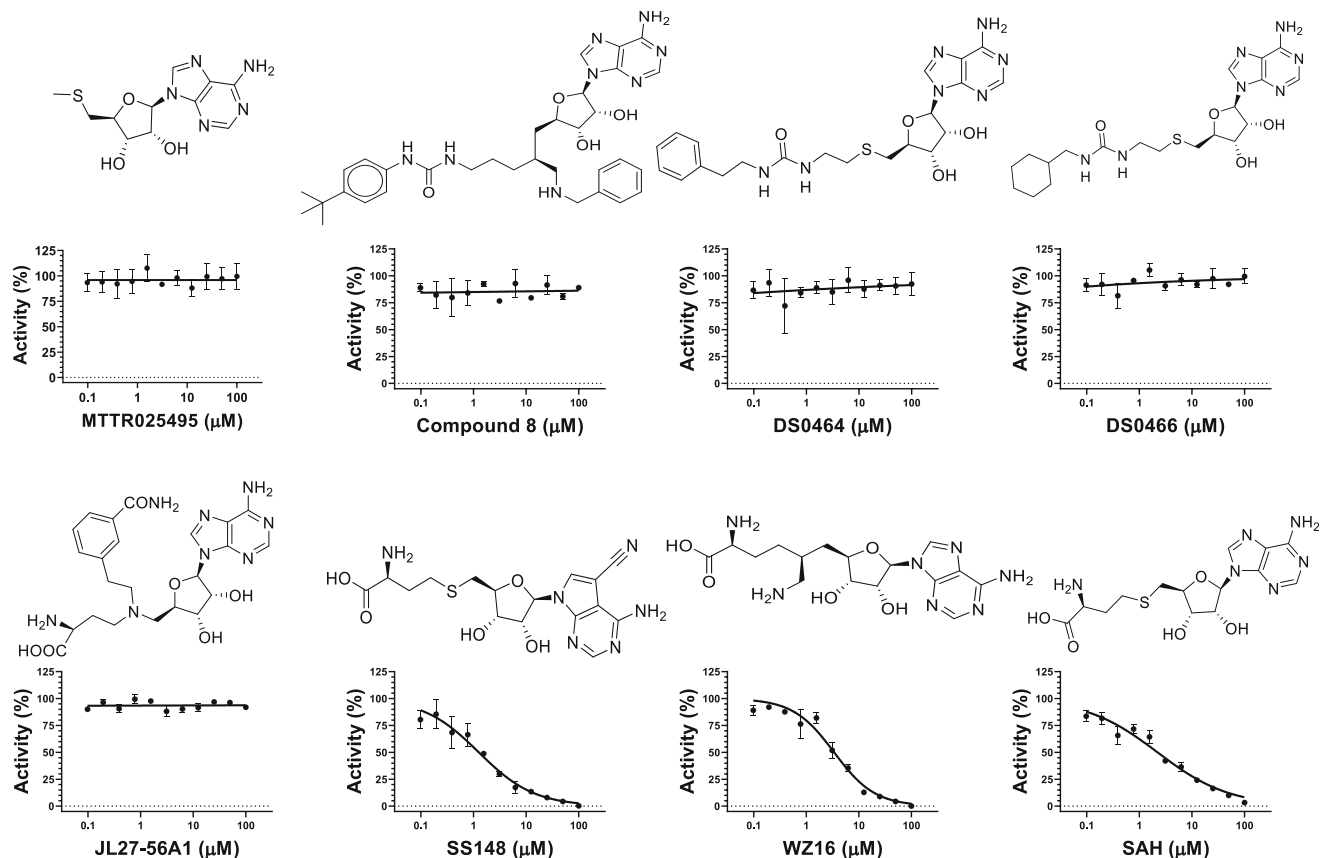


FIGURE 1 Inhibition of nsp10–nsp16 complex MTase activity. Effect of seven previously published⁷ inhibitors of nsp14 MTase activity was tested on nsp10–nsp16 complex methyltransferase activity using the radiometric assay as described in material and methods. Only SS148 and WZ16 inhibited nsp16 complex MTase activity. The structure of each compound is shown above each plot. SAH was used as a control. Experiments were performed in triplicate and IC₅₀ values are presented in Table 1

TABLE 1 Inhibition of nsp10–nsp16 MTase activity

Compound	IC ₅₀ (μM)	Hill slope
SS148	1.2 ± 0.4	0.9 ± 0.4
WZ16	3.4 ± 0.7	1.2 ± 0.2
SAH	2.2 ± 0.2	0.6 ± 0.1

Note: Values are from Figure 1 and are presented as mean ± SD from triplicate experiments (N = 3).

± 0.4 and 3.4 ± 0.7 μM, respectively (Figure 1 and Table 1). An IC₅₀ value of 2.2 ± 0.2 μM was determined for SAH as a control.

2.2 | Crystal structures

To uncover the atomic details of the nsp10–nsp16 interactions with SS148 and WZ16, we performed the crystallographic analysis of the nsp10–nsp16/SS148 and nsp10–nsp16/WZ16 complexes. The nsp10–nsp16/SS148 and nsp10–nsp16/WZ16 crystals belonged to the trigonal

P3₁21 space group and diffracted to the 2.9 and 2.8 Å resolution, respectively. The nsp10–nsp16/SS148 (PDB ID: 7R1T) and nsp10–nsp16/WZ16 (PDB ID: 7R1U) structures were subsequently solved by molecular replacement and further refined to good R factors and geometry as summarized in Table S1. One molecule of the nsp10–nsp16 complex and one molecule of the ligand (either SS148 or WZ16) per asymmetric unit were present, thereby confirming the 1:1:1 nsp10:nsp16:ligand stoichiometry. Both ligands were bound to the SAM-binding site of nsp16 as expected (Figure 2a,c). The binding of these ligands to the nsp10–nsp16 complex was mediated by multiple interactions including both direct (via Asn43, Gly71, Gly73, Asp99, Leu100, Asn101, Asp114, Cys115, and Asp130) and indirect water-mediated hydrogen bonds (via Asn43, Ala72, and Thr82; Figure 2b,d).

In the case of the nsp10–nsp16/WZ16 complex, an additional electron density in the m7GpppA-binding site of nsp16 was observed, corresponding to a dinucleoside triphosphate. Since the nsp10–nsp16 protein complex was not supplemented with such dinucleoside triphosphate during the crystallization experiment, it had to

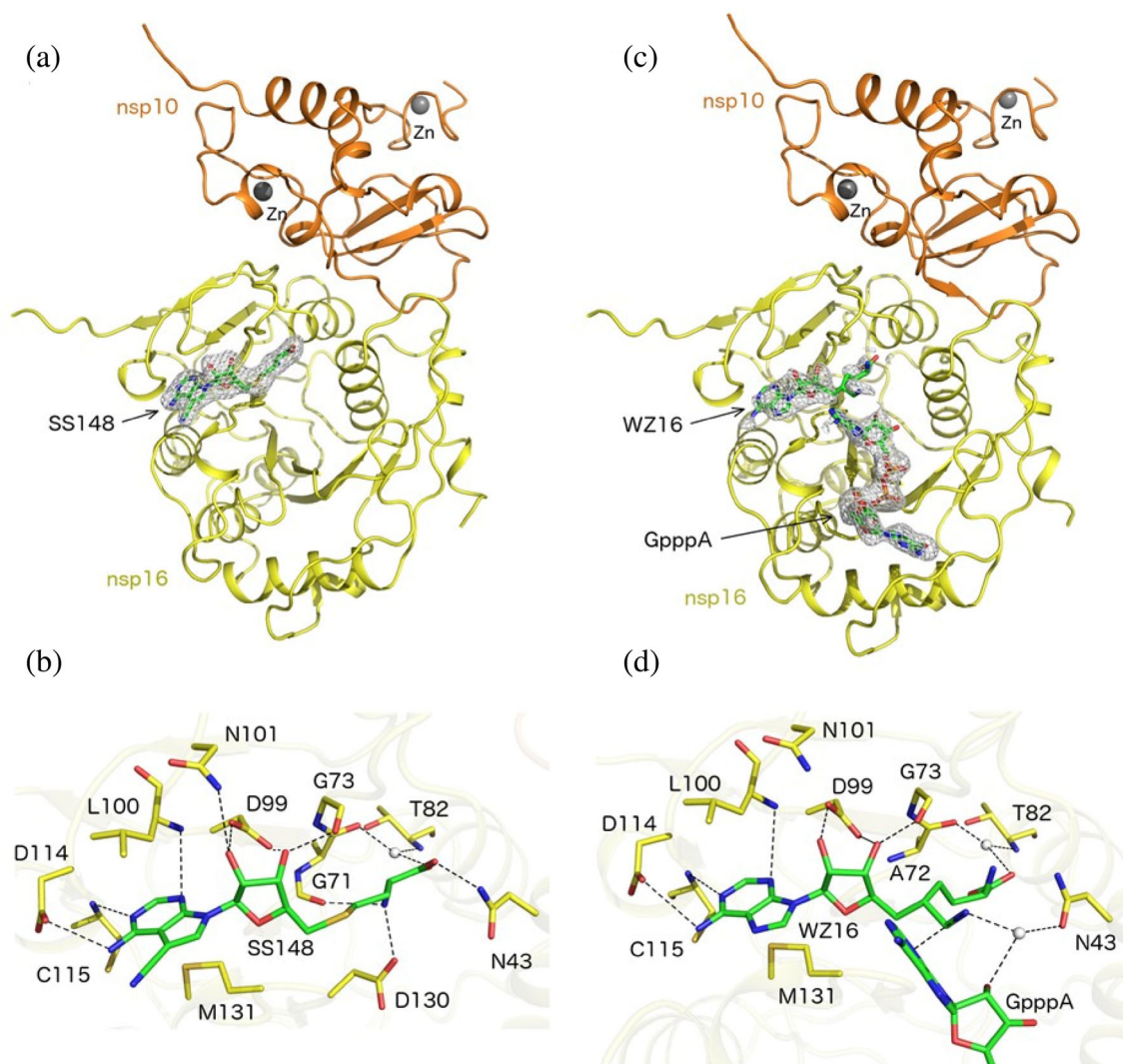


FIGURE 2 Crystal structures of the SARS-CoV-2 nsp10–nsp16 2'-O-RNA methyltransferase in complex with the SS148 (PDB ID: 7R1T) and WZ16 (PDB ID: 7R1U) inhibitors. (a) Overall view of the nsp10–nsp16/SS148 complex. The protein backbone is shown in cartoon representation; the nsp16 and nsp10 proteins are depicted in yellow and orange, respectively. The SS148 ligand is shown in stick representation and colored according to elements: carbon, green; nitrogen, blue; oxygen, red; phosphorus, orange; sulfur, yellow. The unbiased Fo-Fc omit map contoured at 3σ is shown around the SS148 ligand. (b) Detailed view of the SS148 ligand binding site. The SS148 ligand and side chains of selected nsp10–nsp16 amino acid residues are shown in stick representation with carbon atoms colored according to the protein assignment and other elements colored as in (a). Water molecules are shown as gray spheres; hydrogen atoms are not shown. Selected hydrogen bonds involved in the nsp10–nsp16/SS148 interaction are presented as dotted black lines. (c) Overall view of the nsp10–nsp16/WZ16 complex, depicted as in (a). The unbiased Fo-Fc omit map contoured at 2σ is shown around the WZ16 ligand and around the putative GpppA dinucleoside triphosphate. (d) Detailed view of the WZ16 ligand binding site, depicted as in (b)

originate from *Escherichia coli* and co-isolated with the nsp16 protein during purification of the protein from bacteria. GpppA, ApppA, and mApppA are the most abundant dinucleoside triphosphates involved in capping of RNA in *E. coli*,²⁸ and the m7GpppA-capped RNA is the natural substrate of the viral nsp10–nsp16 2'-O-RNA MTase. Therefore, we modeled GpppA in the observed electron density (Figure 2c). GpppA fitted well in the electron density, however, we cannot exclude that a mixture of several dinucleoside triphosphates species was

present. The dinucleoside triphosphate bound to the nsp10–nsp16–WZ16 complex was located at the same position and was bound through identical interactions as the RNA cap analog, m7GpppA, previously co-crystallized with the nsp10–nsp16–SAM complex (PDB ID: 6WKS).²⁷ No such dinucleoside triphosphate was observed in the structure of the nsp10–nsp16/SS148 complex, tempting us to speculate that the nsp10–nsp16–WZ16 and nsp10–nsp16–GpppA interactions were cooperative and mutually stabilizing.

Both SS148 and WZ16 compounds are structurally related to SAM/SAH and bind to the SAM/SAH-binding site of nsp16 through similar interactions. When compared with SAH, SS148 contains a nitrile group bound to the C7-position of the 7-deaza-adenine heterocyclic moiety. Nevertheless, the mechanism of its binding to nsp16 is essentially the same as SAH (Figures 2b and S1d). The WZ16 compound contains an additional aminomethyl group bound to a carbon atom replacing the sulfur atom in the structure of SAH. This aminomethyl group forms both direct and indirect water-mediated hydrogen bonds with the dinucleoside triphosphate and with the Asn43 residue of nsp16 (Figure 2d). These interactions may stabilize the nsp16–GpppA–WZ16 ternary complex.

2.3 | Mechanism of action of inhibitors

To further explore the mode of binding biochemically, we determined the mechanism of action (MOA) of SS148 and WZ16 by determining IC_{50} values for each compound at various concentrations of one substrate while keeping the second substrate at a fixed concentration as previously

described.²⁹ Potential SAM competition of WZ16 and SS148 was evaluated by IC_{50} determination at K_m of RNA substrate (1 μM) and varying concentrations (0.4–10 μM) of 3H -SAM. A linear increase in IC_{50} values was observed as the concentration of SAM in the assay was increased, indicating a SAM competitive pattern of inhibition for both SS148 and WZ16 (Figure 3a,c). Increase in the concentration of RNA substrate at fixed SAM concentration (10 μM ; $5x K_m SAM$) had no effect on IC_{50} values for SS148, indicating an apparent non-competitive pattern of inhibition with respect to RNA (Figure 3b). For WZ16 however, a significant decrease in IC_{50} values was observed as the RNA concentration was increased at fixed SAM concentration of 10 μM ($5x K_m SAM$), presenting a pattern of uncompetitive inhibition with regards to RNA. This indicates that RNA can bind first, and its binding increases the affinity of WZ16 for binding to nsp10–nsp16 complex (Figure 3d). This is consistent with our structural observation that WZ16 was co-crystallized with a batch of nsp16 protein that carried RNA cap through protein expression and purification. We previously observed and reported a pattern of inhibition for (R)-PFI-2, a potent and selective inhibitor of human SETD7 MTase, in which the

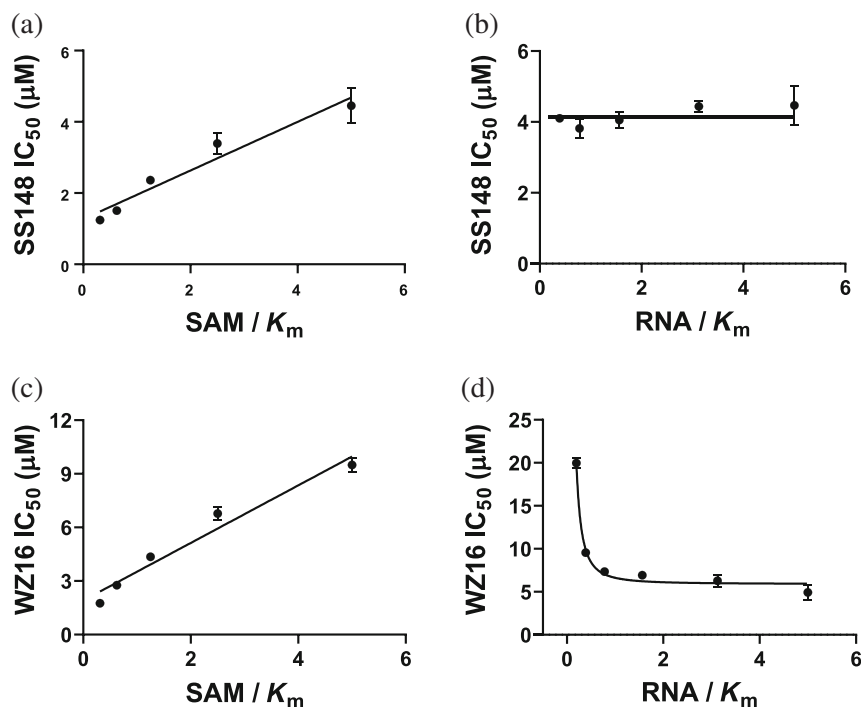


FIGURE 3 Mechanism of action (MOA) of inhibitors. (a, c) IC_{50} values were determined at a fixed concentration of RNA substrate at $K_m RNA$ (1 μM) and varying concentrations of SAM (up to 10 $\mu M/5x K_m SAM$). Linear correlation of the increase in IC_{50} values and the increase in SAM concentration indicated a SAM competitive pattern of inhibition. (b, d) IC_{50} values were also determined at varying concentrations of RNA (up to 5 μM ; $5x K_m RNA$) and fixed 10 μM of SAM ($5x K_m SAM$). The experiments were performed in triplicate ($N = 3$) and IC_{50} values are presented as mean \pm SD. A pattern of noncompetitive inhibition with respect to RNA (b; no change in IC_{50} values as the concentration of RNA increased) was observed with SS148, indicating RNA binding does not affect SS148 binding. An uncompetitive pattern of inhibition with respect to RNA (d; the decrease in IC_{50} values as the RNA concentration increased) indicated that the binding of RNA can increase affinity of WZ16 in a concentration-dependent manner

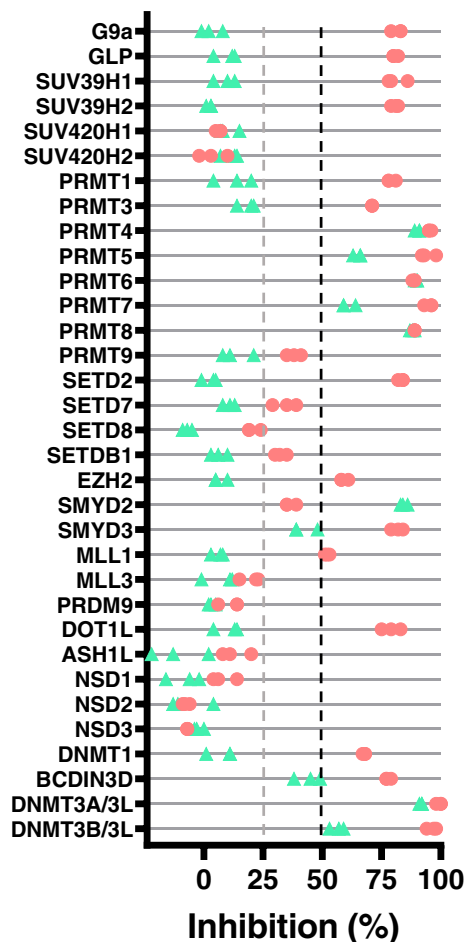


FIGURE 4 Comparison of WZ16 and SAH inhibition of human MTases. Selectivity of (▲) WZ16 against 33 human protein arginine, lysine, RNA and DNA methyltransferases was tested at 20 μ M in parallel with assessing the inhibition of the same proteins by (●) SAH (the product of the reaction) at the same concentration (20 μ M). The black- and gray-dashed lines indicate the 50% and 25% inhibition cut off, respectively. Experiments were performed in triplicate as described previously³¹

competition of the inhibitor with one substrate (peptide) was significantly affected by the concentration of the other (SAM) substrate.³⁰ The mechanism that WZ16 binding would be affected by RNA concentration is consistent with its co-crystallization in the presence of cap RNA.

2.4 | Selectivity of SS148 and WZ16

Selectivity of WZ16 against 33 human protein arginine (PRMTs) and lysine (PKMTs) MTases, and BCDIN3D (an RNA MTase) and DNA MTases (DNMTs) was assessed as we previously described for SS148 selectivity assay.^{7,31} WZ16 was selective against G9a, GLP, SUV39H1, SUV39H2, SUV420H1, SUV420H2, PRMT1, PRMT3, PRMT9, SETD2, SETD7, SETD8, SETDB1,

EZH2, SMYD3, MLL1, MLL3, PRDM9, DOT1L, ASH1L, NSD1, NSD2, NSD3, DNMT1, and BCDIN3D, but inhibited MTase activity of protein arginine MTases (PRMT4, PRMT5, PRMT6, PRMT7, and PRMT8), DNMT3a, DNMT3b, and SMYD2 by more than 50% at 20 μ M (Figure 4 and Table S2). We previously reported a similar pattern of PRMT inhibition for SS148.⁷

Inhibition of MTase activities by the product of the MTase reaction, SAH, is well established.³² As WZ16 and SS148 are structurally very similar to SAH, we decided to test if their patterns of inhibition of human MTases are also similar to that of SAH at the same concentration. This would also clarify the usefulness of these compounds to optimize towards more selective dual inhibitors of nsp14–nsp16 MTase activities. We therefore tested the inhibition by SAH at 20 μ M on all 33 human MTases (Figure 4 and Table S2). Interestingly, WZ16 was a lot more selective against human MTases at 20 μ M than SAH, indicating suitability of these compounds for further optimization to improve potency, selectivity, and cell permeability.

3 | CONCLUSION

SARS-CoV-2 nsp10–nsp16 complex is an RNA MTase involved in RNA cap formation, enabling the virus to evade the immune system in humans. To our knowledge, only nonselective nanomolar inhibitors of nsp16 have been reported to-date.³³ Although the MTase active site of nsp14 and nsp16, the two SARS-CoV-2 MTases, are quite different (Figure S1), our cross-screening of inhibitors of nsp14 MTase activity against nsp10–nsp16 resulted in identifying SS148 and WZ16 as nsp16 MTase inhibitors. Our structural and biochemical assays elucidated a new mechanism of RNA-dependent SAM-competitive inhibition. SAH binds to a groove on the surface of nsp16 or into a tunnel of nsp14. Although these binding sites to some extent have a similar shape, they are surrounded by different amino acid residues, except for nsp14 D352 that corresponds to nsp16 D99 (Figure S1). Identifying potent compounds that function as dual inhibitors of nsp14 and nsp16 MTase activities, could lead to efficient prevention of coronavirus RNA cap formation and vulnerability of coronaviruses to the immune system of humans.

4 | MATERIALS AND METHODS

4.1 | IC₅₀ determination against nsp10–nsp16

The *in vitro* activity of SARS-CoV-2 nsp10–nsp16 was measured as previously reported.⁹ Various concentrations

of compounds (final concentrations of 0.098–100 μM) were mixed with 125 nM of nsp16 complex (1:8 ratio of nsp16:nsp10) and 0.8 μM biotinylated-RNA (5' N7-meGpppACCCCC-biotin) in the reaction buffer containing 50 mM Tris (pH 7.5), 100 mM KCl, 5 mM DTT, 0.01% Triton X-100, 0.01% bovine serum albumin, and 1.5 mM MgCl_2 . The reactions were then started by adding 1.7 μM ^3H -SAM and were allowed to progress for 30 min at room temperature (23°C). The signal was detected using standard SPA plate protocol. Final dimethyl sulfoxide (DMSO) concentration was 5%. SAH and DMSO were used as controls. The data were analyzed using GraphPad Prism 9.

4.2 | Mechanism of action studies

The MOA of WZ16 and SS148 was determined by measuring the IC_{50} values of WZ16 and SS148 for nsp10–nsp16 complex at a fixed concentration of RNA substrate at $K_{\text{m RNA}}$ (1 μM) and varying concentrations of SAM (up to 10 μM /5x $K_{\text{m SAM}}$), and at varying concentrations of RNA (up to 5 μM ; 5x $K_{\text{m RNA}}$) and fixed concentration (10 μM) of SAM (5x $K_{\text{m SAM}}$). The experiments were performed in triplicate ($N = 3$). The data were analyzed using GraphPad Prism 9.

4.3 | Protein expression and purification for crystallography

The truncated SARS-CoV-2 nsp10 protein (residues 10–131) and full-length nsp16 protein (residues 1–298) were expressed as fusion proteins with N-terminal 8x histidine (His_8) purification tags followed by SUMO solubility and folding tags using our previously established protocols.²⁶ Briefly, the proteins were expressed separately in the *E. coli* BL21 DE3 NiCo bacterial strain (New England Biolabs) in the LB medium supplemented with 25 μM ZnSO_4 . The protein expression was induced at optical density of 0.6 with 150 μM isopropyl-1-thio-D-galactopyranoside and the proteins were expressed overnight at 18°C. Bacterial cells were harvested by centrifugation and lysed using the Emulsiflex C3 instrument (Avestin) in the lysis buffer (50 mM Tris pH 8, 300 mM NaCl, 5 mM MgSO_4 , 20 mM imidazole, 10% glycerol, 3 mM β -mercaptoethanol). The lysate was precleared by centrifugation for 30 min at 30,000g and incubated with the HisPur Ni-NTA Superflow agarose (Thermo Fisher Scientific) for 30 min. Then, the agarose beads were extensively washed with the lysis buffer and the proteins of interest were eluted with the lysis buffer supplemented with 300 mM imidazole. The SUMO–nsp10 and SUMO–

nsp16 fusion proteins were mixed in equimolar amounts and then, the His_8 -SUMO tags were removed by overnight cleavage with the recombinant yeast Ulp1 protease. The nsp10–nsp16 complex was further purified using the size exclusion chromatography at the HiLoad 16/600 Superdex 75 prep grade column (Cytiva) in the storage buffer (10 mM Tris pH 7.4, 150 mM NaCl, 5% glycerol, 1 mM TCEP) followed by the reverse Ni-NTA affinity chromatography at the HisTrap HP column (Cytiva). The purified nsp10–nsp16 protein complex was concentrated to 4 mg/mL, aliquoted, flash frozen in liquid nitrogen, and stored at 193 K.

For biochemical assays, the nsp10–nsp16 complex was purified as described before.⁹

4.4 | Crystallization and crystallographic analysis

For the crystallographic analysis, the nsp10–nsp16 protein complex was supplemented with either SS148 or WZ16 compound at a final concentration of 1 mM. The protein crystals were obtained within 3–5 days in the sitting drops consisting of 400 nL of the protein complex and 200 nL of the well solution using the vapor diffusion method at 291 K. The nsp10–nsp16/SS148 crystals were grown using the well solution composed of 10% PEG 20,000, 20% PEG MME 550, 30 mM NaNO_3 , 30 mM Na_2HPO_4 , 30 mM $(\text{NH}_4)_2\text{SO}_4$, and 100 mM MES/imidazole pH 6.5, whereas the nsp10–nsp16/WZ16 crystals were grown using the well solution composed of 8% PEG 8,000, 200 mM NaCl, and 100 mM MES pH 6. Upon harvest, the crystals were cryoprotected in the well solution supplemented with 20% glycerol and cooled in liquid nitrogen. The crystallographic datasets were collected from single crystals. The nsp10–nsp16/SS148 dataset was collected on the BL14.1 beamline at the BESSY II electron storage ring operated by the Helmholtz-Zentrum Berlin,³⁴ whereas the nsp10–nsp16/WZ16 dataset was collected using the home source, Rigaku MicroMax-007 HF rotating anode equipped with the Dectris Pilatus 200 K pixel detector.

The data were integrated and scaled using XDS.³⁵ The structures of the nsp10–nsp16/SS148 and nsp10–nsp16/WZ16 complexes were solved by molecular replacement using the structure of the nsp10–nsp16/sinefungin complex as a search model (PDB ID: 6YZ1).²⁶ The initial model was obtained with Phaser³⁶ from the Phenix package.³⁷ The model was further improved using automatic model refinement with Phenix.refine³⁸ from the Phenix package³⁷ and manual model building with Coot.³⁹ Statistics for data collection and processing, structure solution and refinement are summarized in Table S1. Structural figures were generated with the PyMOL Molecular

Graphics System v2.0 (Schrödinger, LLC). The atomic coordinates and structural factors were deposited in the PDB (<https://www.rcsb.org>).

AUTHOR CONTRIBUTIONS

Martin Klima: Investigation, data curation (equal); formal analysis (equal); validation (equal); writing – original draft (equal); writing – review and editing (equal). **Aliakbar Khalili Yazdi:** Investigation, data curation (equal); formal analysis (equal); writing – original draft (equal); writing – review and editing (equal). **Fengling Li:** Investigation, data curation (equal); formal analysis (equal); writing – original draft (equal); writing – review and editing (equal). **Irene Chau:** Investigation, data curation (equal); formal analysis (equal). **Taraneh Hajian:** Investigation, resources (equal); writing – review and editing (supporting). **Albina Bolotokova:** Resources (supporting); writing – review and editing (supporting). **H. Ümit Kaniskan:** Resources (supporting); writing – review and editing (equal). **Yulin Han:** Resources (supporting); writing – review and editing (supporting). **Ke Wang:** Resources (supporting); writing – review and editing (supporting). **Deyao Li:** Resources (supporting); writing – review and editing (supporting). **Minkui Luo:** Resources (supporting); supervision (supporting); writing – review and editing (supporting). **Jian Jin:** Resources (supporting); supervision (supporting); writing – review and editing (equal). **Evzen Boura:** Formal analysis (equal); funding acquisition (equal); resources (equal); supervision (equal); writing – review and editing (equal). **Masoud Vedadi:** Conceptualization (lead); formal analysis (equal); funding acquisition (equal); supervision (lead); writing – original draft (lead); writing – review and editing (lead).

ACKNOWLEDGMENT

We thank the Helmholtz-Zentrum Berlin für Materialien und Energie for the allocation of synchrotron radiation beamtime. We are grateful to Jiri Brynda for the collection of the nsp10/nsp16/SS148 crystallographic dataset. Structural Genomics Consortium is a registered charity (1097737) that receives funds from Bayer AG, Boehringer Ingelheim, Bristol Myers Squibb, Genentech, Genome Canada through Ontario Genomics Institute [OGI-196], EU/EFPIA/OICR/McGill/KTH/Diamond Innovative Medicines Initiative 2 Joint Undertaking [EubOPEN grant 875510], Janssen, Merck KGaA (aka EMD in Canada and USA), Pfizer and Takeda.

FUNDING INFORMATION

This research was funded by the University of Toronto COVID-19 Action Initiative-2020 (2), COVID-19 Mitacs Accelerate postdoctoral award to A.K.Y., and by European

Regional Development Fund; OP RDE; Project: “Chemical biology for drugging undruggable targets (ChemBioDrug)” [CZ.02.1.01/0.0/0.0/16 019/0000729]. Czech Academy of Sciences [RVO: 61388963] is also acknowledged.

CONFLICT OF INTEREST

The authors declare no potential conflict of interest.

DATA AVAILABILITY STATEMENT

Structures have been deposited in PDB (7R1T and 7R1U).

ORCID

Evzen Boura  <https://orcid.org/0000-0002-9652-4065>

Masoud Vedadi  <https://orcid.org/0000-0002-0574-0169>

REFERENCES

- Horova V, Landova B, Hodek J, et al. Localization of SARS-CoV-2 capping enzymes revealed by an antibody against the nsp10 subunit. *Viruses*. 2021;13(8):1487–1497.
- Nencka R, Silhan J, Klima M, et al. Coronavirus RNA-methyltransferases: Function, structure and inhibition. *Nucleic Acids Res*. 2022;50(2):635–650.
- Eckerle LD, Becker MM, Halpin RA, et al. Infidelity of SARS-CoV Nsp14-exonuclease mutant virus replication is revealed by complete genome sequencing. *PLoS Pathog*. 2010;6(5):e1000896.
- Bouvet M, Imbert I, Subissi L, Gluais L, Canard B, Decroly E. RNA 3'-end mismatch excision by the severe acute respiratory syndrome coronavirus nonstructural protein nsp10/nsp14 exonuclease complex. *Proc Natl Acad Sci U S A*. 2012;109(24):9372–9377.
- Feder M, Pas J, Wyrwicz LS, Bujnicki JM. Molecular phylogenetics of the RrmJ/fibrillarin superfamily of ribose 2'-O-methyltransferases. *Gene*. 2003;302(1–2):129–138.
- Zust R, Cervantes-Barragan L, Habjan M, et al. Ribose 2'-O-methylation provides a molecular signature for the distinction of self and non-self mRNA dependent on the RNA sensor Mda5. *Nat Immunol*. 2011;12(2):137–143.
- Devkota K, Schapira M, Perveen S, et al. Probing the SAM binding site of SARS-CoV-2 Nsp14 in vitro using SAM competitive inhibitors guides developing selective Bisubstrate inhibitors. *SLAS Discov*. 2021;26(9):1200–1211.
- Perveen S, Khalili Yazdi A, Devkota K, et al. A high-throughput RNA displacement assay for screening SARS-CoV-2 nsp10-nsp16 complex toward developing therapeutics for COVID-19. *SLAS Discov*. 2021;26(5):620–627.
- Khalili Yazdi A, Li F, Devkota K, et al. A high-throughput radioactivity-based assay for screening SARS-CoV-2 nsp10-nsp16 complex. *SLAS Discov*. 2021;26(6):757–765.
- Otava T, Sala M, Li F, et al. The structure-based design of SARS-CoV-2 nsp14 methyltransferase ligands yields Nanomolar inhibitors. *ACS Infect Dis*. 2021;7(8):2214–2220.
- Chen Y, Guo D. Molecular mechanisms of coronavirus RNA capping and methylation. *Viol Sin*. 2016;31(1):3–11.
- Decroly E, Ferron F, Lescar J, Canard B. Conventional and unconventional mechanisms for capping viral mRNA. *Nat Rev Microbiol*. 2011;10(1):51–65.

13. Bujnicki JM, Rychlewski L. Reassignment of specificities of two cap methyltransferase domains in the reovirus lambda 2 protein. *Genome Biol.* 2001;2(9):RESEARCH0038.
14. Egloff MP, Benarroch D, Selisko B, Romette JL, Canard B. An RNA cap (nucleoside-2'-O-)-methyltransferase in the flavivirus RNA polymerase NS5: Crystal structure and functional characterization. *EMBO J.* 2002;21(11):2757–2768.
15. Bouvet M, Debarnot C, Imbert I, et al. *In vitro* reconstitution of SARS-coronavirus mRNA cap methylation. *PLoS Pathog.* 2010; 6(4):e1000863.
16. Decroly E, Debarnot C, Ferron F, et al. Crystal structure and functional analysis of the SARS-coronavirus RNA cap 2'-O-methyltransferase nsp10/nsp16 complex. *PLoS Pathog.* 2011; 7(5):e1002059.
17. Chen Y, Su C, Ke M, et al. Biochemical and structural insights into the mechanisms of SARS coronavirus RNA ribose 2'-O-methylation by nsp16/nsp10 protein complex. *PLoS Pathog.* 2011;7(10):e1002294.
18. Benoni R, Krafcikova P, Baranowski MR, Kowalska J, Boura E, Cahova H. Substrate specificity of SARS-CoV-2 Nsp10-Nsp16 Methyltransferase. *Viruses.* 2021;13(9):1722.
19. Aouadi W, Blanjoie A, Vasseur JJ, Debart F, Canard B, Decroly E. Binding of the methyl donor S-adenosyl-l-methionine to Middle East respiratory syndrome coronavirus 2'-O-Methyltransferase nsp16 promotes recruitment of the allosteric activator nsp10. *J Virol.* 2017;91(5):e02217-16.
20. Rosas-Lemus M, Minasov G, Shuvalova L, et al. High-resolution structures of the SARS-CoV-2 2'-O-methyltransferase reveal strategies for structure-based inhibitor design. *Sci Signal.* 2020;13(651):eabe1202.
21. Joseph JS, Saikatendu KS, Subramanian V, et al. Crystal structure of nonstructural protein 10 from the severe acute respiratory syndrome coronavirus reveals a novel fold with two zinc-binding motifs. *J Virol.* 2006;80(16):7894–7901.
22. Matthes N, Mesters JR, Coutard B, et al. The non-structural protein Nsp10 of mouse hepatitis virus binds zinc ions and nucleic acids. *FEBS Lett.* 2006;580(17):4143–4149.
23. Lugari A, Betzi S, Decroly E, et al. Molecular mapping of the RNA cap 2'-O-methyltransferase activation interface between severe acute respiratory syndrome coronavirus nsp10 and nsp16. *J Biol Chem.* 2010;285(43):33230–33241.
24. Dostalík P, Krafcikova P, Silhan J, et al. Structural analysis of the OC43 coronavirus 2'-O-RNA Methyltransferase. *J Virol.* 2021;95(15):e0046321.
25. Lin S, Chen H, Ye F, et al. Crystal structure of SARS-CoV-2 nsp10/nsp16 2'-O-methylase and its implication on antiviral drug design. *Signal Transduct Target Ther.* 2020;5(1):131.
26. Krafcikova P, Silhan J, Nencka R, Boura E. Structural analysis of the SARS-CoV-2 methyltransferase complex involved in RNA cap creation bound to sinefungin. *Nat Commun.* 2020; 11(1):3717.
27. Viswanathan T, Arya S, Chan SH, et al. Structural basis of RNA cap modification by SARS-CoV-2. *Nat Commun.* 2020; 11(1):3718.
28. Hudecek O, Benoni R, Reyes-Gutierrez PE, et al. Dinucleoside polyphosphates act as 5'-RNA caps in bacteria. *Nat Commun.* 2020;11(1):1052.
29. Copeland RA. Evaluation of enzyme inhibitors in drug discovery. John Wiley & Sons, Inc., New Jersey, USA 2005.
30. Barsyte-Lovejoy D, Li F, Oudhoff MJ, et al. (R)-PFI-2 is a potent and selective inhibitor of SETD7 methyltransferase activity in cells. *Proc Natl Acad Sci U S A.* 2014;111(35):12853–12858.
31. Scheer S, Ackloo S, Medina TS, et al. A chemical biology toolbox to study protein methyltransferases and epigenetic signaling. *Nat Commun.* 2019;10(1):19.
32. Talukdar A, Mukherjee A, Bhattacharya D. Fascinating transformation of SAM-competitive protein Methyltransferase inhibitors from nucleoside analogues to non-nucleoside analogues. *J Med Chem.* 2022;65(3):1662–1684.
33. Bobileva O, Bobrovs R, Kanepe I, et al. Potent SARS-CoV-2 mRNA cap Methyltransferase inhibitors by Bioisosteric replacement of methionine in SAM Cosubstrate. *ACS Med Chem Lett.* 2021;12(7):1102–1107.
34. Khan AA, Ullah S, Amin R. Correction to: Optimal control analysis of COVID-19 vaccine epidemic model: A case study. *Eur Phys J Plus.* 2022;137(2):198.
35. Kabsch W. XDS. *Acta Crystallogr D Biol Crystallogr.* 2010; 66(Pt 2):125–132.
36. McCoy AJ, Grosse-Kunstleve RW, Adams PD, Winn MD, Storoni LC, Read RJ. Phaser crystallographic software. *J Appl Cryst.* 2007;40(Pt 4):658–674.
37. Liebschner D, Afonine PV, Baker ML, et al. Macromolecular structure determination using X-rays, neutrons and electrons: Recent developments in Phenix. *Acta Crystallogr D Struct Biol.* 2019;75(Pt 10):861–877.
38. Afonine PV, Grosse-Kunstleve RW, Echols N, et al. Towards automated crystallographic structure refinement with phenix. *Refine. Acta Crystallogr D Biol Crystallogr.* 2012;68(Pt 4): 352–367.
39. Emsley P, Cowtan K. Coot: Model-building tools for molecular graphics. *Acta Crystallogr D Biol Crystallogr.* 2004;60(Pt 12 Pt 1):2126–2132.

SUPPORTING INFORMATION

Additional supporting information can be found online in the Supporting Information section at the end of this article.

How to cite this article: Klima M, Khalili Yazdi A, Li F, Chau I, Hajian T, Bolotokova A, et al. Crystal structure of SARS-CoV-2 nsp10–nsp16 in complex with small molecule inhibitors, SS148 and WZ16. *Protein Science.* 2022;31(9): e4395. <https://doi.org/10.1002/pro.4395>